PCCP

Dynamic Article Links

Cite this: *Phys. Chem. Chem. Phys.*, 2012, **14**, 7229–7233

www.rsc.org/pccp

PAPER

Structural and electronic properties of $CuSbS_2$ and $CuBiS_2$: potential absorber materials for thin-film solar cells

Jesse T. R. Dufton, Aron Walsh, Pooja M. Panchmatia, Laurie M. Peter, Diego Colombara and M. Saiful Islam*

Received 19th January 2012, Accepted 27th March 2012
DOI: 10.1039/c2cp40916j

As the demand for photovoltaics rapidly increases, there is a pressing need for the identification of new visible light absorbing materials for thin-film solar cells that offer similar performance to the current technologies based on CdTe and $Cu(In,Ga)Se_2$. Metal sulphides are the ideal candidate materials, but their band gaps are usually too large to absorb significant fractions of visible light. However, by combining Cu^+ (low binding energy d^{10} band) and Sb^{3+}/Bi^{3+} (low binding energy s^2 band), the ternary sulphides $CuSbS_2$ and $CuBiS_2$ are formed, which have been gathering recent interest for solar cell applications. Using a hybrid density functional theory approach, we calculate the structural and electronic properties of these two materials. Our results highlight the stereochemical activity of the Sb and Bi lone pair electrons, and predict that the formation of hole carriers will occur in the Cu d^{10} band and hence will involve oxidation of Cu(I).

1 Introduction

New thin-film solar cell materials and a greater understanding of their properties are needed to meet the urgent demand for sustainable, lower-cost and scalable photovoltaics (PV). The CdTe and $CuIn_{1-x}Ga_xSe_yS_{2-y}$ (CIGS) absorber systems have been developed for thin-film PV devices, but may be limited in the long-term by the scarcity of Te, Ga, and In.[1–5] There is therefore an increasing need to expand the range of absorber materials that are available as viable alternatives to the toxic Cd in CdTe and the relatively expensive CIGS based systems. One of the main advantages of these inorganic thin-film materials over silicon is that they absorb light more strongly because the optical transition is spatially direct rather than requiring simultaneous absorption or emission of photons.[1]

Recently, Cu_2ZnSnS_4 (CZTS) has attracted considerable interest as a promising absorber material with suitable optical properties (near-optimum direct band-gap energy of 1.5 eV; large absorption coefficient of 10^4 cm^{-1}), as well as containing earth-abundant elements.[6–8] However, there are challenges with the CZTS system related to structural polymorphism and control of the precise cation stoichiometry.

Alternative ternary copper sulfides based on Cu–Bi–S or Cu–Sb–S type materials[9–18] such as $CuBiS_2$ and $CuSbS_2$ show promising properties as absorber materials for thin-film solar cells, as well as containing abundant and non-toxic elements. An early study of Rodriguez-Lazcano *et al.*[18] reported a method to produce $CuSbS_2$ thin films through a solid state reaction involving thin films of Sb_2S_3 and CuS. Rabhi *et al.*[17] have studied the structural, optical and electrical properties of $CuSbS_2$ thin films grown by thermal evaporation and have related the effects of substrate heating conditions on these properties. Manolache *et al.*[12] have examined the influence of precursor concentration on the morphology and the structure of $CuSbS_2$ thin films obtained from aqueous solutions. However, in the case of $CuBiS_2$ and $CuSbS_2$, their fundamental properties and performance have not been fully characterized. Indeed, it is clear that the underlying bulk and electronic structure of ternary copper sulfide materials are complex, but are crucial to the greater understanding of their structure-property relationships and PV behavior.

The present study uses first-principles Density Functional Theory (DFT) techniques to investigate key issues related to bulk structure, band gaps and local electronic structure of lone pairs in the $CuBiS_2$ and $CuSbS_2$ materials, with reference to experimental results where possible. This work extends analogous computational studies of other thin film PV materials[19–22] including CZTS,[23,24] and provides a solid platform for further experimental characterisation.

2 Methods

Density functional theory (DFT) calculations were performed utilizing the plane-wave projector augmented-wave (PAW) method[25,26] using the Vienna *ab initio* simulation package (VASP).[27,28] For the exchange–correlation functional, the generalized gradient approximation (GGA) of Perdew–Burke–Ernzerhof (PBE)[29] was used along with the Heyd-Scuseria-Ernzerhof (HSE06)[30] hybrid-functional where exact

Department of Chemistry, University of Bath, Bath, UK BA2 7AY. E-mail: M.S.Islam@bath.ac.uk

Hartree–Fock exchange replaces 25% of the exchange potential of the PBE functional. For studies of photoactive materials where the band gap is a critical material property, it is important that there is an accurate description of the band gap and the states at the band edges. The use of hybrid functionals is found to be important as standard GGA functionals significantly underestimate the band gap of a wide range of semiconducting materials.[19,24] It should be noted that calculations were also performed with the PBE0[31] hybrid functional. However we found that the screened exchange provided by the HSE06 functional gave the most accurate reproduction of experimental band gap values, whereas PBE0 tended towards overestimation. We should also note that recent GGA-PBE calculations[32] reported a small band gap of 0.5 eV for $CuBiS_2$, although the focus of this study was the thermoelectric performance at ambient temperature of the hole-doped system.

Structural and electronic properties have been determined by modelling the 16 atom crystallographic unit cell. For total energy calculations, a plane-wave energy cut-off of 300 eV has been used throughout. The infinite solid is modelled using standard periodic boundary conditions in three dimensions. For sampling of the Brilloiun zone, a 4 × 6 × 2 Monkhorst–Pack[33] *k*-point mesh has been used, which offered good convergence in the calculated structural and thermodynamic properties. All lattice parameters and ionic positions were fully relaxed by minimising the forces and total energy of the system. A residual atomic force tolerance of $<1 \times 10^{-4}$ eV Å^{-1} was used, a stringent convergence criteria. Similar DFT methods have been successfully applied to copper-sulphide type compounds,[23,24] and other energy-related materials.[34–36]

3 Results and discussion

3.1 Crystal structures and band gaps

$CuSbS_2$ (chalcostibite) and $CuBiS_2$ (emplectite) are isostructural (orthorhombic space group *Pnma*). The structures are composed of square pyramidal MS_5 units (M = Sb/Bi) which edge share to form continuous MS_2 units aligned with the *b* axis. These continuous units are separated by CuS_4 tetrahedra (shown in Fig. 1) so that the base of the square pyramidal units are aligned to face one another, thus directing the Sb/Bi lone pair electron density into the void separating the MS_5 units.

In order to assess the accuracy of our computational approach, structural optimisations of $CuSbS_2$ and $CuBiS_2$ were performed based on the experimental bulk crystal structures and using both PBE and the HSE06 hybrid functional. In Table 1 and 2 we compare our calculated lattice parameters and band gaps to experimental studies. We find that standard DFT utilizing the PBE functional describes the lattice parameters adequately for both $CuSbS_2$ and $CuBiS_2$. There is a slight over-estimation of the *a* lattice parameter ($\approx$2%) in both systems, which is likely to be due to an under-estimation of the lone pair–lone pair interactions (*i.e.* the lack of dynamic correlation). However more importantly we find that, as is the case for other chalcogenide systems, the band gap is severely underestimated using a GGA functional.[19,23]

The use of the HSE06 hybrid functional improves the reproduction of lattice parameters and we no longer observe a slight over estimation of the *a* lattice parameter for either system. But crucially the use of this hybrid functional improves the reproduction of the band gaps dramatically, as found in DFT studies of CZTS.[24] As noted, an accurate description of the band gap is crucial in designing new PV materials with improved absorption properties. Several experimental band gaps for $CuSbS_2$ have been published; and we have included the values published by Zhou *et al.*[15] and Rodriguez-Lazcano *et al.*[18] in Table 1. Of the published experimental values our results support the value of 1.52 eV of Rodriguez-Lazcano *et al.* This also accords with an approximate band gap energy of 1.5 eV from recent studies of $CuSbS_2$ thin films formed *via* chalcogenisation of Sb–Cu metal precursors.[40]

For $CuBiS_2$, the calculated band gap of 1.55 eV (using HSE06) is in good accord with the experimental value of 1.65 eV,[38] and falls in the range for a viable absorber material. The differences between experimental values could be due to variations in sample quality or incorrect linear interpolation in deriving the band gap energy. Clearly synthetic conditions and

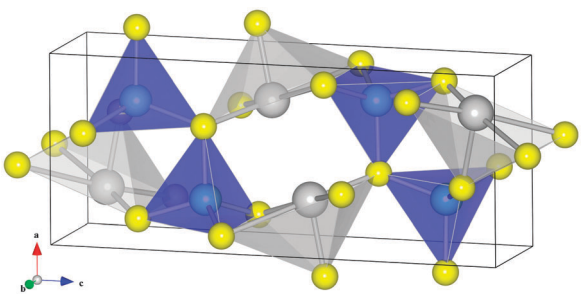

Fig. 1 Structure of $CuMS_2$ (where M = Sb or Bi) showing CuS_4 tetrahedra (blue), MS_5 square pyramidal units (grey) and S atoms (yellow).

Table 1 Comparison of calculated $CuSbS_2$ lattice parameters and band gaps with experiment

		PBE		HSE06	
Parameter	Expt	Calc	Δ (Expt-Calc)	Calc	Δ (Expt-Calc)
a/Å	6.016[a]	6.137	0.121	6.055	−0.039
b/Å	3.797[a]	3.834	0.038	3.807	−0.010
c/Å	14.499[a]	14.480	−0.019	14.523	−0.024
$\alpha = \beta = \gamma$ (°)	90.0[a]	90.0	0	90.0	0
E_g (eV)	1.38[a]; 1.52[b]	0.90	—	1.69	—

[a] Zhou *et al.*[15] [b] Rodriguez *et al.*[18]

Table 2 Comparison of calculated $CuBiS_2$ lattice parameters and band gaps with experiment

		PBE		HSE06	
Parameter	Expt	Calc	Δ (Expt-Calc)	Calc	Δ (Expt-Calc)
a/Å	6.134[a]	6.263	0.129	6.178	0.044
b/Å	3.911[a]	3.949	0.038	3.924	0.012
c/Å	14.549[a]	14.498	−0.051	14.568	−0.019
$\alpha = \beta = \gamma$ (°)	90.0[a]	90.0	0.0	90.0	0.0
E_g (eV)	1.65[b]; 1.8[c]	0.36	—	1.55	—

[a] Kyono *et al.*[37] [b] Pawar *et al.*[38] [c] Sonawane *et al.*[39]

the presence/absence of secondary phases must affect the band gap measured by experimental groups significantly. For both $CuSbS_2$ and $CuBiS_2$ the fundamental band gaps are predicted to be indirect in nature; however, the difference between the lowest energy direct and indirect gaps is only of the order of 0.1 eV, so that a strong onset of optical absorption is still expected. This is distinct from the case of Si, where the difference is larger than 2 eV, which limits the absorption of visible light in thin films.

3.2 Thermodynamic stability

Evaluation of the phase stability of new PV compounds is of great importance for the design of effective synthetic routes. Issues such as elemental losses during thermal treatments,[40,41] as well as compatibility of components at the interfaces,[42] are currently faced in various fields of materials science and technology. A recent study[43] has stressed the significance of thermochemistry in the understanding and prediction of the chemical equilibria of PV materials. Hence, knowledge of the thermodynamic functions of new materials for device application is crucial. Currently no sound experimental measurement is available for either $CuSbS_2$ or $CuBiS_2$. In these circumstances, computation is a viable option for the provision of such data. We have therefore calculated the enthalpy of formation for each compound with respect to their elemental standard. The total energy for the reactions

$$Cu(s) + Sb(s) + 2S(s) \rightarrow CuSbS_2 \quad (1)$$

and

$$Cu(s) + Bi(s) + 2S(s) \rightarrow CuBiS_2 \quad (2)$$

is −1.08 eV and −1.16 eV, respectively at the level of HSE06. This suggests that the materials are thermodynamically stable, and the values are comparable to other metal sulphide materials.[44] Further studies are required to estimate the complete chemical potentials and their temperature dependence, for direct applications in thermochemical studies.

3.3 Density of states

Fig. 2 shows the orbital-projected density of states (DOS) for $CuSbS_2$ and $CuBiS_2$. It is clear that the electronic structure of the two materials is very similar. We see prominent peaks corresponding to the S-3*s* states from −18 to −14 eV. Peaks comprised mainly of Sb-5*s*/Bi-6*s* states, with this peak in $CuSbS_2$ from −11.5 to −9.5 eV and in $CuBiS_2$ from −13 to −10 eV, this peak off-set being the most notable difference between the density of states of the two materials. We then observe a series of intense peaks which make up the valence band; as is the case for many other chalcogenide PV materials *e.g.* CZTS, $CuInS_2$, $CuGaS_2$, $CuInSe_2$, the top of the valence band is dominated by Cu-3*d* states.[23,24,45] This is clearly illustrated in Fig. 3 which shows the calculated charge density for the valence and conduction bands of $CuSbS_2$. It should be stressed that the corresponding charge density figure for $CuBiS_2$ has been omitted since it is almost identical. We also find that the conduction band is comprised of hybridized (Sb-5*s*/S-3*p*)/(Bi-6*s*/S-3*p*) states, analogous to the (Sn-5*s*/S-3*p*) states seen in CZTS.

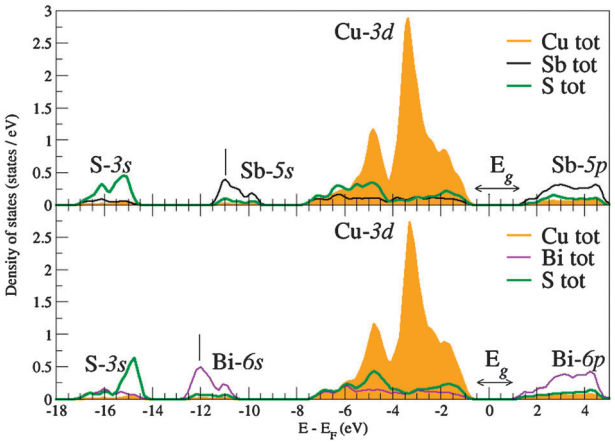

Fig. 2 Orbital-projected density of states for $CuSbS_2$ (top) and $CuBiS_2$ (bottom) indicating the Cu, Sb, Bi and S states.

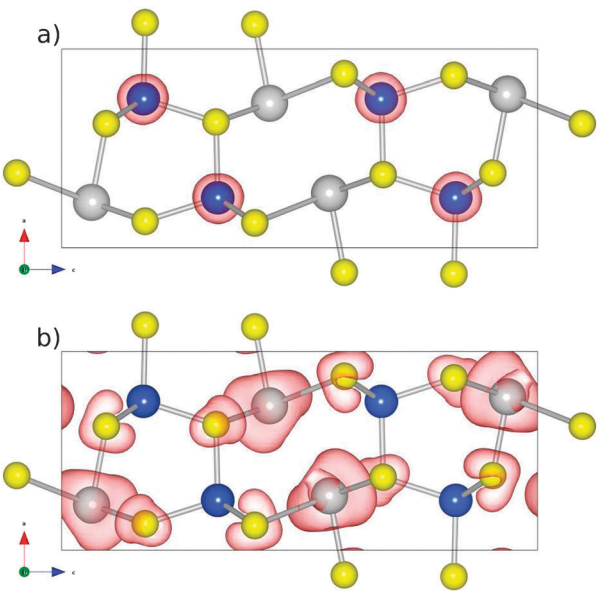

Fig. 3 Charge density calculated for (a) the top of the valence band (E–E_F = −3.5 → 0 *eV*) and (b) the bottom of the conduction band (E–E_F = 1 → 5 *eV*) in $CuSbS_2$. Colours are similar to Fig. 1; Cu (blue), Sb (grey), S (yellow), charge density (red).

As Cu in $CuSbS_2$ and $CuBiS_2$ exists as Cu^+ (d^{10}) the Cu-3*d* states of the valence band are fully occupied and we do not find Cu states in the conduction band. Fig. 2 shows that the top of the valence band is comprised mostly of Cu-3*d* states. Therefore upon photoexcitation the promotion of a Cu based electron will result in the oxidation of Cu^+ (d^{10}) to Cu^{2+} (d^9). This may have implications for hole transport in $CuSbS_2$, as films from parallel experimental work have been shown to be slightly Cu poor.[17,40] We note that intrinsic ionic defects (such as Cu vacancies) are not the focus of this study, but is an area that is of current investigation.

3.4 Local structural environment

The majority of PV materials are based around regular tetrahedral networks at the atomic level (zinc-blende or wurtzite crystal structures). A comprehensive understanding of the

structure and bonding in $CuSbS_2$ and $CuBiS_2$, due to their low symmetry structures, will be necessary in order to describe the surface and interfacial properties that will be key in the design and optimisation of improved photovoltaic devices.

When we compare the local environment of the MS_5 (M = Sb/Bi) square pyramids we find considerable local distortion. The Sb/Bi ions are not centrally located within the basal plane of the MS_5 square pyramids as one might expect based on Valence Shell Electron Pair Repulsion (VSEPR) theory.[46] The structural distortions arise as a result of electronic effects relating to the Sb/Bi lone pairs.

Considering the structural deformations, we find that in $CuSbS_2$ the distorting effect of the stereoactive lone pair causes more structural distortion than in $CuBiS_2$, as measured by the standard deviation (σ) of the M–S bond lengths and S–M–S angles listed in Table 3, where we also find good agreement with the experimental values. As with the experimental work of Kyono *et al.*[37] we observe that the Sb 5s lone pair seems to be more stereochemically active in terms of repelling the neighbouring Cu than the Bi 6s lone pair; the M–Cu distance is very similar in the two materials, 3.414 Å and 3.422 Å for $CuSbS_2$ and $CuBiS_2$ respectively. This result is despite the discrepancy between the ionic radii of Sb and Bi. Interestingly this does not lead to the CuS_4 tetrahedra being more distorted in $CuSbS_2$ (Table 4). In fact the CuS_4 tetrahedra in $CuBiS_2$ are more irregular, but the deviations are much less significant than those in the MS_5 square pyramids.

Turning to the cause of the distortion of the MS_5 square pyramids, we have already noted that VSEPR theory is unable to provide an explanation. Essentially this is because VSEPR assumes a classical model of the lone pair(s) in the system, in which the s^2 electrons occupy a non-bonding orbital, and electrostatics control the coordination. Instead we can adopt the revised lone pair model of Walsh *et al.*,[47] which has been used to rationalise the presence of lone pair induced structural distortions in other systems *e.g.* PbO and SnO.

In this revised model the s^2 lone pair electrons are no longer assumed to reside within a non-bonding orbital. They interact with valence band anion (S) *p* states and the resulting hybrids can be seen at the bottom (bonding) and top (antibonding) of the valence band. In certain systems where this antibonding orbital has considerable *s* character it is possible for the antibonding orbital to hybridize with the cation (Sb/Bi) *p* states. However this interaction cannot take place in undistorted structures as it is symmetry forbidden, consequently where this cation *p*–antibonding hybridization offers significant stabilization the structure distorts removing the symmetry constraint.

Table 3 Bond lengths, angles and standard deviation (σ) in the MS_5 square pyramids where M = Sb/Bi

	$CuSbS_2$	$CuBiS_2$
Bond lengths (Å)		
Mean M–S (calc)	2.759	2.821
σ (calc)	0.325	0.288
σ (expt)	0.329	0.303
Bond angles (deg)		
Mean S–M–S (calc)	89.47	90.39
σ (calc)	8.47	7.32
σ (expt)	8.48	7.29

Table 4 Bond lengths, angles and standard deviation (σ) in the CuS_4 tetrahedra

	$CuSbS_2$	$CuBiS_2$
Bond lengths (Å)		
Mean Cu–S (calc)	2.330	2.342
σ (calc)	0.010	0.024
σ (expt)	0.010	0.021
Bond angles (deg)		
Mean S–Cu–S (calc)	109.47	109.44
σ (calc)	1.863	2.048
σ (expt)	1.757	1.957

The electron density of the stabilized antibonding orbital forms a distorted lobe which is projected into the structural void like a classic lone pair.

When considering how this revised lone pair model can be applied to $CuSbS_2$ and $CuBiS_2$ it is helpful to consult Fig. 4 which shows the partial density of states in the valence and conduction bands for both materials. Looking first at the partial density of states for $CuSbS_2$ we can see a set of small peaks with an energy of −3 eV. These show the interaction of the (Sb-5*s*/S-3*p*)* orbital with the Sb-5*p* which as discussed above gives the stabilisation requiring structural distortion. When we visualise the orbitals present at this particular energy we clearly see the distorted lobe of electron density present as a result of this stabilised antibonding orbital, shown in Fig. 5.

If we now consider $CuBiS_2$ we find that the peaks in Fig. 4 are less pronounced. This can be rationalised as the binding

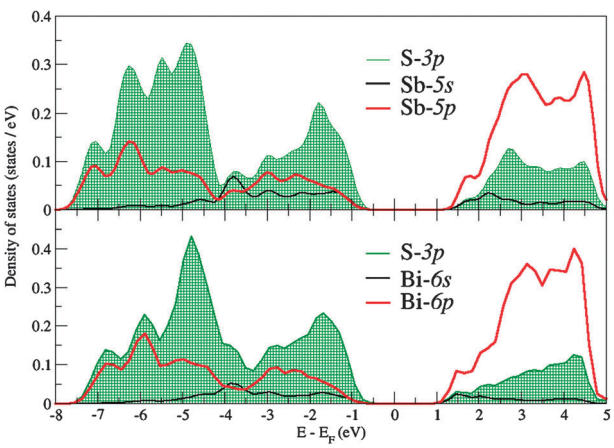

Fig. 4 Partial orbital-projected density of states for $CuSbS_2$ (top) and $CuBiS_2$ (bottom).

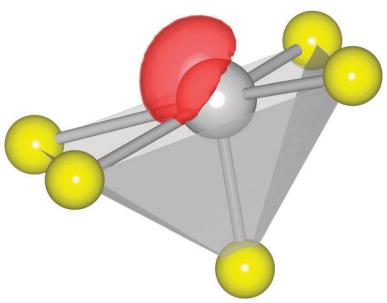

Fig. 5 SbS_5 square pyramid with lone pair electron density shown in red, Sb in grey and S in yellow.

energy of the Bi-6s orbital is lower than that of the Sb-5*s*. Consequently the energies of the Bi-6*s* and S-3*p* are not as well matched as the Sb-5*s* and S-3*p* are. Therefore the resulting (Bi-6*s*/S-3*p*)* hybrid does not possess as much s orbital character as the (Sb-5*s*/S-3*p*)* hybrid. This indicates that the stabilisation available from interaction with the Bi-6*p* states is lower than that in $CuSbS_2$. These results help to rationalize the increased degree of structural distortion in $CuSbS_2$ in which the stabilization afforded by such distortion is greater than in $CuBiS_2$.

4 Conclusions

The present study of $CuSbS_2$ and $CuBiS_2$ has used quantum chemical techniques to provide deeper fundamental insight into the electronic and local structural properties, which are of direct relevance to their use as absorber materials for thin-film solar cells.

The following main findings emerge from our investigations, which provide a strong basis for further characterization and optimization of these materials. (1) The calculations show excellent reproduction of the observed crystal structures of $CuSbS_2$ and $CuBiS_2$ including the unusual SbS_5 and BiS_5 coordination geometry. (2) A calculated band gap energy of 1.69 eV for $CuSbS_2$ which agrees with the available experimental data, although this accord only occurs with the use of the HSE06 hybrid functional. For $CuBiS_2$ we predict a band gap of 1.55 eV that falls in the optimum range for a viable absorber material. (3) The results highlight the stereochemical activity of the Sb and Bi lone pair electrons rationalizing the asymmetric environment around Sb and Bi. (4) The density of states of both $CuSbS_2$ and $CuBiS_2$ indicate that the formation of hole carriers will occur in the Cu d^{10} band and hence will involve oxidation of Cu(I).

Further simulation work will include detailed studies of the defect and dopant properties of these materials.

Acknowledgements

We thank the EPSRC Supergen PV-21 consortium for financial support. The computations were run on the HECToR facilities *via* the Materials Chemistry Consortium. All figures were produced with the aid of VESTA.[48]

References

1 L. M. Peter, *Philos. Trans. R. Soc. London, Ser. A*, 2011, **369**, 1840–1856.
2 M. Gratzel, *Philos. Trans. R. Soc. London, Ser. A*, 2007, **365**, 993–1005.
3 A. Romeo, A. Terheggen, D. Abou-Ras, D. Batzner, F. Haug, M. Kalin, D. Rudmann and A. Tiwari, *Progr. Photovolt.: Res. Appl.*, 2004, **12**, 93–111.
4 D. Ginley, M. A. Green and R. Collins, *MRS Bull.*, 2008, **33**, 355–364.
5 J. Schmidtke, *Opt. Express*, 2010, **18**, A477–A486.
6 J. J. Scragg, P. J. Dale and L. M. Peter, *Electrochem. Commun.*, 2008, **10**, 639–642.
7 K. Ito and T. Nakazawa, *Jpn. J. Appl. Phys.*, 1988, **27**, 2094–2097.
8 T. K. Todorov, K. B. Reuter and D. B. Mitzi, *Adv. Mater.*, 2010, **22**, 1.
9 H. Li, Q. Zhang, A. Pan, Y. Wang, B. Zou and H. J. Fan, *Chem. Mater.*, 2011, **23**, 1299–1305.
10 F. Mesa, G. Gordillo, T. Dittrich, K. Ellmer, R. Baier and S. Sadewasser, *Appl. Phys. Lett.*, 2010, **96**, 082113.
11 F. Mesa, A. Dussan and G. Gordillo, *Phys. Status Solidi C*, 2010, **7**, 917–920.
12 S. Manolache, A. Duta, L. Isac, M. Nanu, A. Goossens and J. Schoonman, *Thin Solid Films*, 2007, **515**, 5957–5960.
13 N. J. Gerein and J. A. Haber, *Chem. Mater.*, 2006, **18**, 6297–6302.
14 F. Mesa, A. Dussan and G. Gordillo, *Phys. B*, 2009, **404**, 5227–5230.
15 J. Zhou, G.-Q. Bian, Q.-Y. Zhu, Y. Zhang, C.-Y. Li and J. Dai, *J. Solid State Chem.*, 2009, **182**, 259–264.
16 S. C. Ezugwu, F. I. Ezema and P. U. Asogwa, *Chalcogenide Lett.*, 2010, **7**, 369–376.
17 A. Rabhi, M. Kanzari and B. Rezig, *Thin Solid Films*, 2009, **517**, 2477–2480.
18 Y. Rodriguez-Lazcano, M. Nair and P. Nair, *J. Cryst. Growth*, 2001, **223**, 399–406.
19 H. Xiao, J. Tahir-Kheli and I. W. A. Goddard, *J. Phys. Chem. Lett.*, 2011, **2**, 212–217.
20 D. O. Scanlon and G. W. Watson, *Appl. Phys. Lett.*, 2010, **97**, 131904.
21 J. Pohl and K. Albe, *J. Mol. Catal. A: Chem.*, 2010, **328**, 023509.
22 Y. Seminovski, P. Palacios and P. Wahnon, *Thin Solid Films*, 2011, **519**, 7517–7521.
23 J. Paier, R. Asahi, A. Nagoya and G. Kresse, *Phys. Rev. B*, 2009, **79**, 115126.
24 S. Chen, X. G. Gong, A. Walsh and S.-H. Wei, *Appl. Phys. Lett.*, 2009, **94**, 036601.
25 P. Blochl, *Phys. Rev. B*, 1994, **50**, 17953–17979.
26 G. Kresse and D. Joubert, *Phys. Rev. B*, 1999, **59**, 1758–1775.
27 G. Kresse and J. Furthmuller, *Comput. Mater. Sci.*, 1996, **6**, 15–50.
28 G. Kresse and J. Furthmuller, *Phys. Rev. B*, 1996, **54**, 11169–11186.
29 J. P. Perdew, K. Burke and M. Ernzerhof, *Phys. Rev. Lett.*, 1996, **77**, 3865–3868.
30 J. Heyd, G. Scuseria and M. Ernzerhof, *J. Chem. Phys.*, 2003, **118**, 8207–8215.
31 J. Perdew, M. Emzerhof and K. Burke, *J. Chem. Phys.*, 1996, **105**, 9982–9985.
32 D. Parker and D. J. Singh, *Phys. Rev. B*, 2011, **83**, 233206.
33 H. Monkhorst and J. Pack, *Phys. Rev. B: Solid State*, 1976, **13**, 5188–5192.
34 A. R. Armstrong, C. Lyness, P. M. Panchmatia, M. S. Islam and P. G. Bruce, *Nat. Mater.*, 2011, **10**, 223–229.
35 M. S. Islam, *Philos. Trans. R. Soc. London, Ser. A*, 2010, **368**, 3255–3267.
36 A. Walsh, K.-S. Ahn, S. Shet, M. N. Huda, T. G. Deutsch, H. Wang, J. A. Turner, S.-H. Wei, Y. Yan and M. M. Al-Jassim, *Energy Environ. Sci.*, 2009, **2**, 774–782.
37 A. Kyono and M. Kimata, *Am. Mineral.*, 2005, **90**, 162–165.
38 S. Pawar, A. Pawar and P. Bhosale, *Bull. Mater. Sci.*, 1986, **8**, 423–426.
39 P. Sonawane, P. Wani, L. Patil and T. Seth, *Mater. Chem. Phys.*, 2004, **84**, 221–227.
40 D. Colombara, L. M. Peter, K. D. Rogers, J. D. Painter and S. Roncallo, *Thin Solid Films*, 2011, **519**, 7438–7443.
41 A. Weber, R. Mainz and H. W. Schock, *J. Appl. Phys.*, 2010, **107**, 013516.
42 Z. Yang, K. Meinhardt and J. Stevenson, *J. Electrochem. Soc.*, 2003, **150**, A1095–A1101.
43 D. Colombara, L. Peter, K. Rogers and K. Hutchings, *J. Solid State Chem.*, 2012, **186**, 36–46.
44 S. Chen, J.-H. Yang, X. G. Gong, A. Walsh and S.-H. Wei, *Phys. Rev. B*, 2010, **81**, 245204.
45 M. G. Brik, *J. Phys.: Condens. Matter*, 2009, **21**, 485202.
46 R. Gillespie and R. Nyholm, *Q. Rev. Chem. Soc.*, 1957, **11**, 339–380.
47 A. Walsh, D. J. Payne, R. G. Egdell and G. W. Watson, *Chem. Soc. Rev.*, 2011, **40**, 4455–4463.
48 K. Momma and F. Izumi, *J. Appl. Crystallogr.*, 2011, **44**, 1272–1276.